Similarity of Scalar Fields in the Convective Boundary Layer

ZBIGNIEW SORBJAN

Department of Physics, Marquette University, Milwaukee, Wisconsin

(Manuscript received 19 March 1998, in final form 3 August 1998)

ABSTRACT

The paper investigates similarity of scalar fields in a horizontally homogeneous, cloud-free, shearless, convective mixed layer. The concept of the ''bottom-up'' and ''top-down'' decomposition is verified for both passive and active scalars, based on a number of large eddy simulations. The bottom-up diffusion is not confirmed to be countergradient. The top-down scaling, based on the values of entrainment fluxes, is found to be inefficient. Alternative sets of scales are proposed and validated for mean values of scalars. For the bottom-up process, the ''free-convective'' scaling is applied. For the top-down processes, new scales are based on the maximum values of scalar gradients in the interfacial layer. The bottom-up and top-down similarity functions for passive and active scalars are found equal.

1. Introduction

Over four decades ago, Monin and Obukhov formulated their milestone surface layer similarity theory (Monin and Obukhov 1954). Since then a simple and effective framework of this approach has found many practical applications in experimental analysis of surface layer turbulence, as well as in parameterization of mass and energy exchange across the earth's surface (e.g., Sorbjan 1989). The success of the Monin–Obukhov (M–O) theory in the surface layer has raised natural questions, such as whether the upper portion of the boundary layer also has a self-similar structure, and whether this structure can be expressed in terms of an equally simple and elegant approach. The positive answer to these questions in the case of the moderately stable boundary layer was found by Nieuwstadt (1984), who introduced the local (height dependent) similarity scales. Based on these local scales, the M–O similarity functions for various statistical moments, spectra, and cospectra, could be simply extended for the entire stably stratified boundary layer (e.g., Sorbjan 1986, 1988a,b, 1989).

An extension of the surface similarity in the convective boundary layer has been found to be more difficult. The first attempt in this direction was undertaken by Deardorff (1970), who introduced the mixed layer scales (hereafter referred to as the ''D scaling'') $w^* = (\beta z_i H_0)^{1/3}$ for velocity, $\theta^* = H_0/w^*$ for the virtual potential temperature, $c^* = Q_0/w^*$ for a passive scalar, and z_i for height, where H_0 is the surface virtual potential temperature flux, Q_0 is the surface scalar flux, $\beta = g/T_0$ is the buoyancy parameter, and z_i is the height of the mixed layer. The mixed layer scaling allowed matching data points from atmospheric measurements, numerical simulations, and tank experiments. Unfortunately, the mixed layer scaling for passive and active scalars was unable to properly handle the effects of entrainment at the top of the mixed layer. Moreover, in contrast to the M–O similarity, no theoretical predictions could be obtained regarding the universal form of the statistical moments in the mixed layer.

In order to account for processes near the bottom and the top of the mixed layer, Wyngaard (1984), Wyngaard and Brost (1984), and Moeng and Wyngaard (1984) developed the concept of ''top-down'' and ''bottom-up'' decomposition for passive and active fields. Consequently, scalar fields were separated into the contributions dependent on the bottom and top fluxes. Deardorff's velocity scale w^* was retained as a universal scale in the entire mixed layer. For a passive scalar, $c^* = Q_0/w^*$ was adopted as a scale for the bottom-up process. In the top-down process, a new scale, $C^* = Q_i/w^*$, was introduced, where Q_i is the passive scalar flux at the top of the mixed layer. Analogous scales, $\theta^* = H_0/w^*$ (for the bottom-up case) and $\Theta^* = H_i/w^*$ (for the top-down case), were applied as the temperature scales. Hereafter, this set of scales (z_i, c^*, C^*, θ^*, Θ^*) will be referred to as the ''W scaling.''

Even though preliminary comparisons of the numerically derived top-down and bottom-up similarity functions with water tank observations (Piper et al. 1995) showed a tentative agreement, the bottom-up–top-down

Corresponding author address: Dr. Zbigniew Sorbjan, Department of Physics, Marquette University, P.O. Box 1881, Milwaukee, WI 53201-1881.
E-mail: sorbjanz@mu.edu

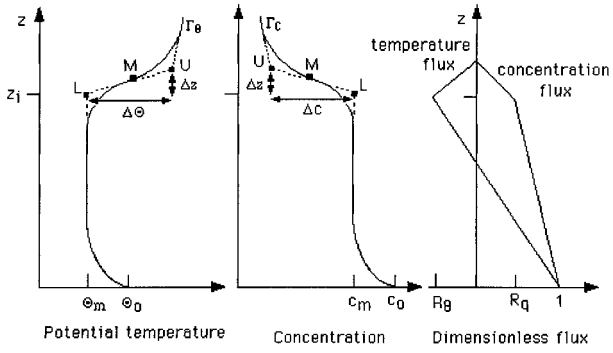

FIG. 1. The schematic structure of the mixed layer (symbols explained in the text).

parameterization has not been sufficiently explored, and a number of unsolved problems remained. For instance, the W scaling has not been adequately tested to be complete and effective, for both passive and active scalars. Therefore, the purpose of this paper is to further investigate the self-similar structure of the convective mixed layer, verify the concept of top-down and bottom-up decomposition for passive as well as for active scalars, and also to validate the convective scaling for mean values of scalars in the lower and the upper portion of the mixed layer. To accomplish these goals, a number of large eddy simulations (LESs) of the atmospheric mixed layer have been performed.

The paper is organized as follows. Diffusion processes for passive scalars are discussed in sections 2 and 3. Convective scales for scalars are introduced in section 4. Dimensionless gradients for passive and active scalars are examined in section 5. The convective similarity in the ''free-encroachment'' regime is elaborated in section 6. A brief description of the large eddy simulation model, and the performed numerical experiments, is given in the appendix.

2. Convective mixing

Let us begin with a general discussion of a horizontally homogeneous, cloud-free, shearless, convective, atmospheric boundary layer, which often persists during the late morning and early afternoon hours over land. With reference to Fig. 1, we will assume that in such a layer, the potential temperature decreases with height, from its surface value Θ_0 to the value Θ_m, which remains constant with height in the mixed layer. At the top of the mixed layer, there is a rapid increase in the potential temperature by $\Delta\Theta$ within a relatively thin interfacial layer of the depth Δz. In the free atmosphere, there is a potential temperature gradient Γ_θ, assumed here to be constant. The turbulent heat flux in the mixed layer linearly decreases with height, from a positive value at the surface to a negative value at the top of the mixed layer z_i. The concentration of a passive scalar and its turbulent flux have analogous distributions. The concentration decreases with height, from its surface value c_0 to the value in the mixed layer c_m. At the top of the mixed layer, there is a rapid increase by Δc.

The increments $\Delta\Theta$, Δc, and Δz in Fig. 1 are defined as $\Delta\Theta = \Theta_U - \Theta_L$, $\Delta c = c_U - c_L$, and $\Delta z = z_U - z_L$, respectively. The subscript U indicates the point where the tangent to the scalar profile at the inflection point M crosses the extension (downward) of the scalar profile in the free atmosphere. The subscript L indicates the point where the tangent to the scalar profile at the inflection point M crosses the extension (upward) of the scalar profile in the mixed layer. It can be noted that from the above definitions it follows that the maximum gradients at the inflection point M are equal to $\Delta\Theta/\Delta z$ or $\Delta c/\Delta z$.

Dispersion of a passive scalar in the mixed layer can be described by the following equation:

$$\frac{\partial c}{\partial t} = -\frac{\partial Q}{\partial z}, \tag{1}$$

where c is the concentration [e.g., specific humidity (g kg^{-1})] and Q is the concentration flux. The considered passive scalar c is associated only with area sources (or sinks) located at the earth's surface and at the top of the mixed layer.

When the scalar is ''well mixed,'' the turbulent concentration flux Q is a linear function of height:

$$Q(z) = Q_0\left(1 - \frac{z}{z_i}\right) + Q_i\frac{z}{z_i}, \tag{2}$$

where Q_0 is the turbulent flux at the surface, and Q_i is the turbulent flux at $z = z_i$. The height of the mixed layer z_i is defined as a level of the minimum heat flux H. Approximately, $z_i = z_L$.

Differentiation of (1), with respect to z, implies that when the concentration flux is linear, that is, when

$$\frac{\partial^2 Q}{\partial z^2} = 0, \tag{3}$$

the concentration gradient $\partial c/\partial z$ is preserved in time (the state hereafter referred to as ''quasi-steady''):

$$\frac{\partial}{\partial t}\left(\frac{\partial c}{\partial z}\right) = 0. \tag{4}$$

Due to linearity of (1) with respect to c and Q, the mixing of a passive scalar in the mixed layer is additive; that is, it can be expressed as a superposition of two processes, bottom-up and top-down (Wyngaard 1984). The first process (hereafter denoted by a subscript ''b'') is associated with a transfer (emission or absorption) of a scalar across the earth's surface. The second process (hereafter denoted by a subscript ''t'') is due to entrainment of a scalar at the top of the mixed layer. Consequently, the mean concentration of the passive scalar and its flux can be decomposed as follows:

$$c = c_b + c_t$$

$$Q = Q_b + Q_t. \tag{5}$$

Based on (3), both the bottom-up and top-down processes can be described by the equations in the form

$$\frac{\partial^2 Q_b}{\partial z^2} = 0$$

$$\frac{\partial^2 Q_t}{\partial z^2} = 0. \tag{6}$$

Just for the sake of general discussion (and not for the purpose of finding a numerical solution), we will close (6) using a simple ''two-scale mixing'' parameterization:

$$Q_b = -k\left(\frac{\partial c_b}{\partial z} - \gamma_{bc}\right)$$

$$Q_t = -k\left(\frac{\partial c_t}{\partial z} - \gamma_{tc}\right), \tag{7}$$

where k is the eddy diffusivity; and γ_{bc} and γ_{tc} are ''countergradient'' correction functions of height (e.g., Deardorff 1966). The terms in (7), proportional to the gradients, represent contributions of smaller eddies, while the terms proportional to γ_{bc} and γ_{tc} reflect the effects of larger eddies (Mahrt 1995). Specifying the boundary conditions, we obtain from (6) and (7)

$$\begin{cases} \dfrac{\partial^2[k(g_{bc} - \gamma_{bc})]}{\partial z^2} = 0 \\ g_{bc} = C\dfrac{c_f}{z} \quad \text{for } z \to 0 \\ g_{bc} = 0 \qquad \text{for } z = z_M \end{cases} \tag{8}$$

and

$$\begin{cases} \dfrac{\partial^2[k(g_{tc} - \gamma_{tc})]}{\partial z^2} = 0 \\ g_{tc} = 0 \qquad \text{for } z \to 0 \\ g_{tc} = \dfrac{\Delta c}{\Delta z} \quad \text{for } z = z_M, \end{cases} \tag{9}$$

where $g_{bc} = \partial c_b/\partial z$ and $g_{tc} = \partial c_t/\partial z$, $c_f = Q_0/u_f$ is the free-convection scalar scale, $u_f = (\beta z H_0)^{1/3}$ is the free-convection velocity scale (Businger et al. 1971), z_M is the height of the inflection point M, and C is a universal constant (of the order of unity).

The lower boundary condition in (8) is assumed to follow the M–O similarity prediction (''$-4/3$ law'') in the free-convective regime. Measurements of Zilitinkevich and Chalikov (1968) confirm this prediction in the surface layer. On the other hand, observations during the Kansas field experiment (Businger et al. 1971) imply that the gradient g_{bc} decreases with height as $z^{-1/2}$. The notation of the lower boundary condition ($z \to 0$) in (8) is symbolic and indicates that the free-convection regime applies only to the upper portion of the surface layer.

It can be noted that the above formulation differs from the approach of Wyngaard (e.g., Wyngaard 1987), who defined the bottom-up and top-down processes based on the values of the scalar flux on the top and the bottom of the mixed layer. In (8) and (9) the bottom-up and top-down processes are based on the values of the gradient on the top and the bottom of the mixed layer. Nevertheless, both formulations are related. The surface flux and the gradient near the surface can be related in terms of the M–O ''free-convection'' formulation [as in the lower boundary condition in (8)], while the flux at the top of the mixed layer and the parameter Δc are expressed by the entrainment rate (Lilly 1968)

$$Q_i = -\Delta c\frac{dz_i}{dt} \tag{10}$$

(no subsidence assumed). The consequences of the formulation (8) and (9) will be further discussed in the next two sections.

3. Bottom-up and top-down diffusion processes for passive scalars

The system (8) describes the bottom-up process, with no scalar entrainment flux across the top of the mixed layer. The system (9) specifies the top-down process, which includes effects of the entrainment flux. It can be noted that within the top-down process, the scalar flux at the top of the mixed layer can be directed upward or downward, depending on the sign of the concentration jump Δc. As a result, hereafter the term top-down will be augmented by the information on the sign of the parameter Δc.

The considered diffusion processes are schematically shown in Fig. 2. In the pure bottom-up case (Fig. 2a), the concentration quickly decreases with height and reaches a constant value in the mixed layer. At the same time, the bottom-up concentration flux decreases linearly from $Q_0 > 0$ at the earth's surface to zero at the top of the mixed layer. In the pure top-down ($\Delta c > 0$) case (Fig. 2b), the concentration in the free atmosphere exceeds the concentration in the mixed layer. The scalar flux decreases linearly with height, from zero at the surface to $Q_i < 0$ at the top of the mixed layer. On the other hand, during the pure top-down ($\Delta c < 0$) case (Fig. 2c), the concentration in the mixed layer is larger than the concentration in the free atmosphere, and the flux increases linearly with height, from zero at the surface to $Q_i > 0$ at the top of the mixed layer. The quasi-steady diffusion of a passive scalar in Fig. 2d ($\Delta c < 0$, $Q_0 > Q_i > 0$) can be represented by the sum of two processes: pure bottom-up ($\Delta c = 0$, $Q_0 > 0$) as in Fig. 2a, and pure top-down ($\Delta c < 0$, $Q_0 = 0$, $Q_i > 0$) as in Fig. 2c. A superposition of processes in Figs. 2b and 2c yields a constant concentration (equal to $2c_0$), and a

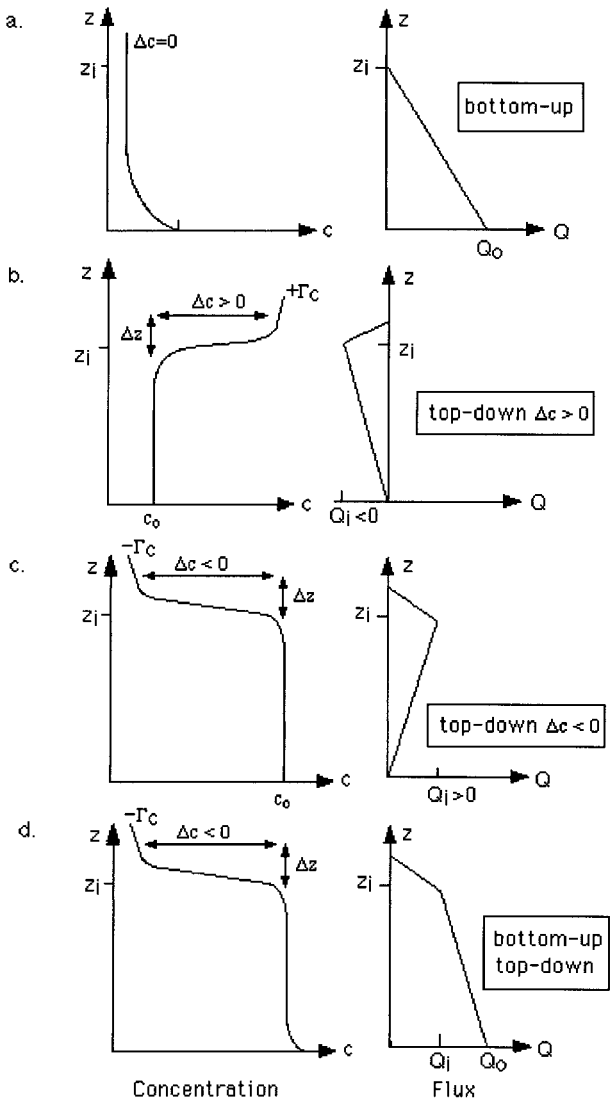

FIG. 2. Schematic profiles of the concentration and the concentration flux for (a) pure bottom-up, (b) pure top-down ($\Delta c > 0$), (c) top-down ($\Delta c < 0$), and (d) bottom-up–top-down ($\Delta c < 0$) processes.

nil concentration flux in the mixed layer, and also above it.

The pure top-down ($\Delta c > 0$) process, with no concentration flux at the earth's surface ($Q_0 = 0$), can easily be generated numerically by beginning the simulation in the quasi-steady mixed layer (obtained during a preliminary run without a passive scalar diffusion). The initial concentration of the passive scalar in the mixed layer should be smaller than in the free atmosphere. Run Pl5b in the Table 1 is an example of a such simulation. A similar simulation was also performed by Wyngaard and Brost (1984). The pure top-down ($\Delta c < 0$) process can be executed in an analogous way, by assuming that the initial concentration in the mixed layer is larger than in the free atmosphere.

The pure bottom-up ($\Delta c = 0$, $Q_0 > 0$) concentration

TABLE 1. Characteristics of the performed LES experiments (the symbols are explained in the appendix).

Run	Mixing process	z_i (m)	Γ_θ (K km^{-1})	w^* (m s^{-1})	θ^* (K)	$\Delta\Theta$ (K)	R_θ	c^* (g kg^{-1})	Δc (g kg^{-1})	R_c	t^* (s)	T/t^*
P00t	Encroachment	1500	0.0	0.789	0.0126	0.0	0.0	0.7890	0.0	0.0	1901	5.2
P15b	Top-down	855	1.5	0.654	0.0153	0.35	−0.17	0.0000	+3.5	$-\infty$	1307	16.8
P52c	Bottom-up	675	3.0	0.605	0.0165	0.6	−0.16	0.1654	+0.05	0.0	1116	14.0
P15a1	Bottom-up–top-down	795	1.5	0.693	0.0157	0.3	−0.17	0.1566	−0.3	+0.05	1244	12.1
P30a	Bottom-up–top-down	645	3.0	0.595	0.0168	0.5	−0.18	0.0168	−0.55	+0.45	1084	11.1
P30a1	Bottom-up–top-down	675	3.0	0.605	0.0165	0.7	−0.18	0.1654	−0.3	+0.05	1116	13.4
P50a	Bottom-up–top-down	615	5.0	0.586	0.0171	0.8	−0.20	0.0171	−0.6	+0.30	1049	14.3
P60a	Bottom-up–top-down	705	3.0	0.614	0.0163	0.5	−0.20	0.1630	−1.5	+0.10	1148	15.7
P15c	Bottom-up–top-down	825	1.5	0.646	0.0155	0.3	−0.17	0.1550	+3.0	−0.30	1277	14.7
P30d	Bottom-up–top-down	675	3.0	0.605	0.0165	0.6	−0.18	0.0165	+0.05	−0.02	1116	13.4
P30c	Bottom-up–top-down	705	3.0	0.614	0.0163	0.6	−0.18	0.1630	+3.2	−0.16	1148	15.6

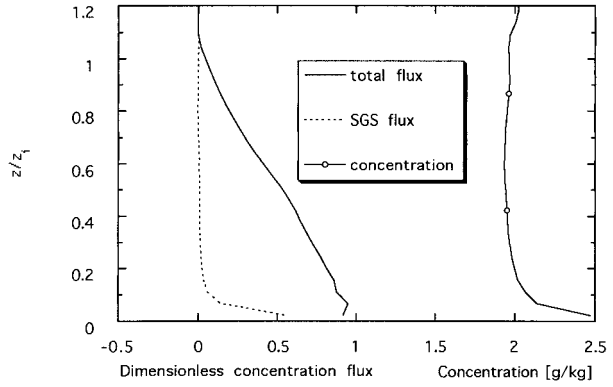

FIG. 3. Profiles of the concentration and its flux (total and subgrid) in the bottom-up process in run P52c.

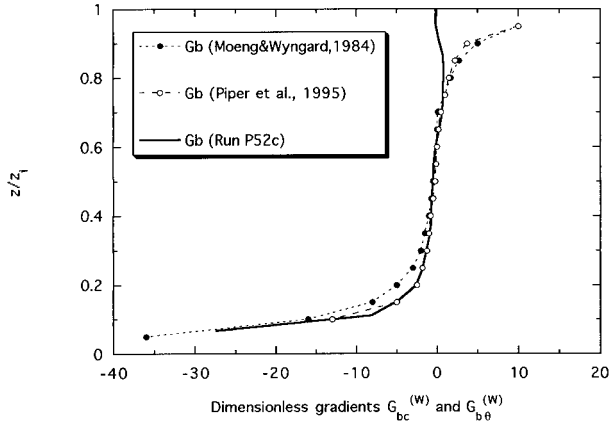

FIG. 4. Comparison of dimensionless gradient $G_{bc}^{(W)} = (z_i/c^*)\partial c/\partial z$ in the pure bottom-up process in run P52c with the results of Moeng and Wyngaard (1984) and Piper et al. (1995).

profile could be generated in two ways. First of all, such a profile could be obtained by a superposition of the bottom-up–top-down ($\Delta c > 0$) (Fig. 2d) and the pure top-down ($\Delta c > 0$) (Fig. 2b) profiles. This would require a numerical simulation with two passive scalars c_1 and c_2. In practice, however, it is much easier to generate the bottom-up process directly, that is, with only one scalar. Run P52c in Table 1 is an example of such a bottom-up simulation. It was executed by emitting a passive scalar through the earth's surface into the quasi-steady mixed layer. The initial concentration profile was assumed to be zero in the mixed layer, and equal to a positive constant (2 g kg^{-1}) in the free atmosphere. While a passive scalar was dispersed in the mixed layer, some of its mass was entrained into the mixed layer from the free atmosphere. This exchange generated a turbulent flux at the top of the mixed layer, expressed by (10). The parameter Δc in (10) decreased in time at about the same rate as the concentration c increased with time. Eventually, the concentration in the mixed layer reached the concentration in the free atmosphere. At this moment, $\Delta c = Q_i = \partial c/\partial z = 0$ at the top of the mixed layer. The resulting pure bottom-up profiles of concentration and its flux are shown in Fig. 3. The figure indicates that the concentration flux is indeed linear, and the concentration is nearly constant above $z/z_i > 0.4$.

Wyngaard and Brost (1984) used a different procedure to generate the pure bottom-up process. They artificially forced the scalar flux to zero at the top of the mixed layer (after each time step). As a consequence, their results at the top of the mixed layer are ''uncertain,'' as pointed out by Moeng and Wyngaard (1984). Simulations described in this paper are free of this flaw.

Fig. 4 presents the dimensionless concentration gradient $G_{bc}^{(W)} = (z_i/c^*)\partial c/\partial z$ (where $c^* = Q_0/w^*$) obtained in the pure bottom-up run P52c. The superscript ''W'' indicates that the W scaling was applied, while the subscripts b and c refer to the bottom-up process for a scalar c. In the same figure, the numerical results of Moeng and Wyngaard (1984) and the tank measurements of Piper et al. (1995) are also displayed. The figure shows that the three curves generally agree in the lower portion of the mixed layer. Near the top of the mixed layer, there is a clear disagreement. The function $G_{bc}^{(W)}$ obtained in run P52c is about zero in this region, in accord with (8). This fact also agrees with the result of Weil (1990) in his Fig. 8c, which was obtained based on a Lagrangian stochastic model, in the case with the skewness $S = 0.5$, and with asymmetric profiles of the second and third moments of the vertical velocity. The functions obtained by Moeng and Wyngaard and by Piper et al. have positive values, which increase with height. The authors associate these positive values with the nonlocal, or countergradient, diffusion at the top of the mixed layer during the bottom-up diffusion.

It should be noted, however, that the functions $G_{bc}^{(W)}$ of Moeng and Wyngaard and of Piper et al. were calculated indirectly. Moeng and Wyngaard obtained $G_{bc}^{(W)}$ by subtracting the dimensionless gradient $\partial c/\partial z$, simulated as the pure top-down process (of their ''red dye''), from the dimensionless gradient $\partial c/\partial z$, simulated as the bottom-up and top-down process (of their ''yellow dye''): $G_{bc}^{(W)} = (z_i/c^*)\partial c/\partial z - (C^*/c^*)G_{tc}^{(W)}$. On the other hand, Piper et al. calculated $G_{bc}^{(W)}$ by subtracting the dimensionless gradient $\partial c/\partial z$, simulated as the top-down process, from the dimensionless gradient $\partial\Theta/\partial z$ for the potential temperature: $G_{bc}^{(W)} = (z_i/\theta^*)\partial\Theta/\partial z - (C^*/\theta^*)G_{tc}^{(W)}$. The indirect calculations of Moeng and Wyngaard, as well as Piper et al., are based on assumptions that the scalar gradients at the top of the mixed layer scale by C^*/z_i and Θ^*/z_i, where $C^* = Q_i/w^*$ and $\Theta^* = H_i/w^*$. As will be shown in section 5, this assumption is not supported by our LES results.

The dimensionless gradient $G_{tc}^{(W)} = (z_i/C^*)\partial c/\partial z$ (where $C^* = Q_i/w^*$) obtained in the top-down run P15b is shown in Fig. 5 (the superscript W indicates that the W scaling was applied, while the subscripts t and c refer to the top-down process for a scalar c). In the same figure, the numerical results of Moeng and Wyngaard (1984), as well as the tank measurements of Piper et al.

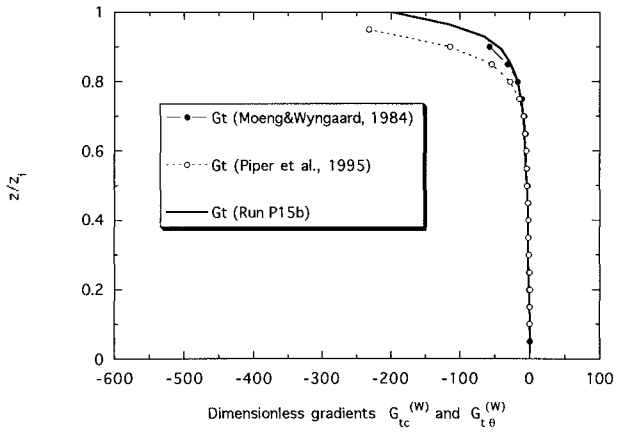

FIG. 5. Comparison of dimensionless gradient $G_{tc}^{(W)} = (z_i/C^*)\partial c/\partial z$ in the bottom-up–top-down ($\Delta c < 0$) process in run P15c with the results of Moeng and Wyngaard (1984) and Piper et al. (1995).

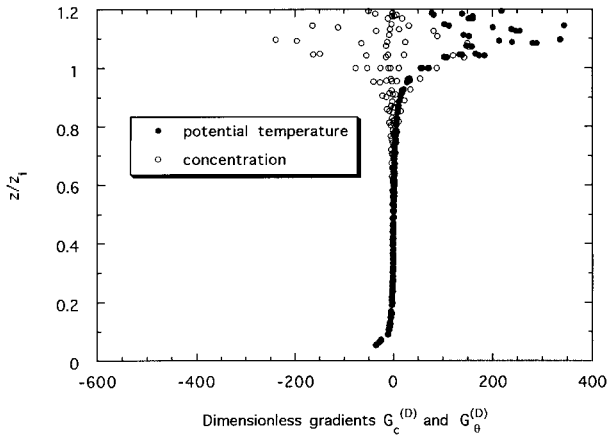

FIG. 6. Dimensionless gradients $G_\theta^{(D)} = (z_i/\theta^*)\partial\Theta/\partial z$ and $G_c^{(D)} = (z_i/c^*)\partial c/\partial z$ obtained from the LES simulations described in the text.

(1996), are also displayed. The top-down function G_t in run P15b agrees with the result of Moeng and Wyngaard, available in the layer $z/z_i < 0.9$. The values obtained by Piper et al. are significantly smaller in the top 20% of the mixed layer.

4. Convective scaling for mean values of scalars

In our search for more effective convective scaling, let us depart from D and W scaling and rewrite Eqs. (8)–(9) in the following dimensionless form:

$$\begin{cases} \dfrac{\partial^2[K_b(G_{bc} - \Gamma_{bc})]}{\partial Z^2} = 0 \\ G_{bc} = C \quad \text{for } Z \to 0 \\ G_{bc} = 0 \quad \text{for } Z = 1 \end{cases} \tag{11}$$

$$\begin{cases} \dfrac{\partial^2[K_t(G_{tc} - \Gamma_{tc})]}{\partial Z^2} = 0 \\ G_{tc} = 0 \quad \text{for } Z \to 0 \\ G_{tc} = 1 \quad \text{for } Z = 1, \end{cases} \tag{12}$$

where the dimensionless gradients are defined as

$$G_{bc} = \frac{z}{c_f}\frac{\partial c_b}{\partial z},$$

$$G_{tc} = \frac{\Delta z}{\Delta c}\frac{\partial c_t}{\partial z}, \tag{13}$$

and $\Gamma_{bc} = \gamma_{bc}z/c_f$, $\Gamma_{tc} = \gamma_{tc}\Delta z/\Delta c$, $K_b = k/(u_f z)$, $K_t = k/(w^*/z_M)$, $Z = z/z_M$, and z_M is the level at which the concentration gradient is maximum and $G_{tc} = 1$.

The above equations are scaled in terms of two different sets of scales. For the bottom-up process [(11)], the free-convective scaling, with z as the height scale and c_f as the scalar scale, is applied. For the top-down process [(12)], Δz is adopted as the height scale and Δc as the mean concentration scale. Analogous parameters, θ_f and $\Delta\Theta$, can be adopted as the temperature scales. We will refer to this new set of scales (z, c_f, θ_f), and (Δz, Δc, $\Delta\Theta$) as the S scaling.

The form of (11)–(12) indicates that the dimensionless gradients G_{bc} and G_{tc} are independent of the boundary conditions. Here G_{bc} and G_{tc} are dependent only on K_b, K_t, Γ_{bc}, and Γ_{tc}. If K_b, K_t, Γ_{bc}, and Γ_{tc} are only functions of Z, G_{bc} and G_{tc} will be unique functions of Z. We will examine this issue in section 5.

It can be noted that the function $G_{tc}^{(W)} = (z_i/C^*)\partial c/\partial z$, defined through the W scaling, can be expressed in terms of the function $G_{tc} = (\Delta z/\Delta c)\partial c_t/\partial z$, defined through the S scaling, and the Richardson number $\mathrm{Ri} = \beta\Delta\Theta z_i/w^{*2} = \Delta\Theta/\theta^*$. Assuming that $dz_i/dt \sim \mathrm{Ri}^{-a}$ and $\Delta z/z_i \sim \mathrm{Ri}^{-b}$, where a and b are both positive and of the order of unity (e.g., Stull 1976; Boers 1989), it can be obtained that $G_{tc}^{(W)} = \mathrm{Ri}^{(a+b)}G_{tc}$. As G_{tc} is expected to be only a function of Z, the derived expression indicates that for given dimensionless height Z, the function $G_{tc}^{(W)}$ should be subjected to a scatter, proportional to $\mathrm{Ri} = \Delta\Theta/\theta^*$. This conclusion will be verified in the next section, based on our large eddy simulations.

5. Dimensionless gradients of the potential temperature and concentration

We shall examine now the three considered sets of scales, D, W, and S. For this purpose, we shall compare the dimensionless gradients for the virtual potential temperature and concentration. The comparison will be based on the results of the large eddy simulations summarized in Table 1 (except run P00t).

Figure 6 depicts the dimensionless gradients for a passive scalar $G_c^{(D)} = (z_i/c^*)\partial c/\partial z$, where superscript D indicates that Deardorff's scaling has been used. In addition, the dimensionless virtual potential temperature gradient $G_\theta^{(D)} = (z_i/\theta^*)\partial\Theta/\partial z$ is also shown. As seen in

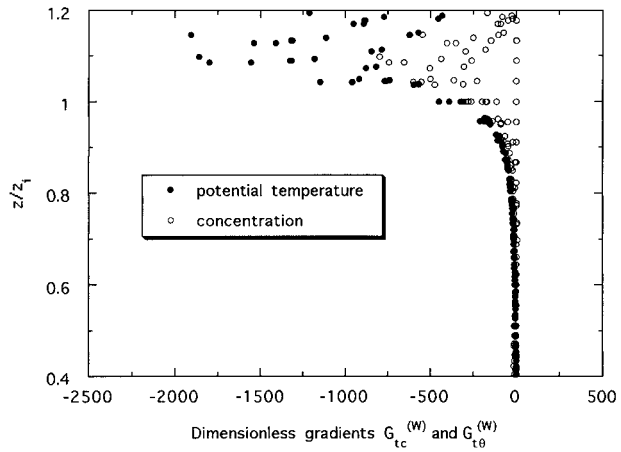

FIG. 7. Dimensionless gradients $G_{t\theta}^{(W)} = (z_i/\Theta^*)\partial\Theta/\partial z$ and $G_{tc}^{(W)} = (z_i/C^*)\partial c/\partial z$ obtained from the LES simulations described in the text.

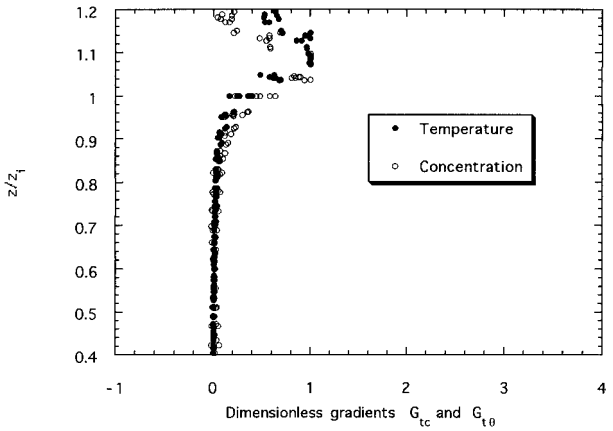

FIG. 8. Dimensionless gradients $G_{t\theta} = (\Delta z/\Delta\Theta)\partial\Theta/\partial z$ and $G_{tc} = (\Delta z/\Delta c)\partial c/\partial z$ obtained from the LES simulations described in the text.

the figure, the boundary layer can clearly be divided into three distinct layers: the ''surface layer,'' the ''mixed layer,'' and the ''entrainment'' layer. In the surface layer, the functions $G_c^{(D)}$ and $G_\theta^{(D)}$ are negative and represented by a single curved line, which quickly increases with height and reaches values near zero at about $z/z_i = 0.1$. In the mixed layer, from about $z/z_i = 0.1$ up to $z/z_i \sim 0.7$, $G_c^{(D)}$ and $G_\theta^{(D)}$ remain near zero. In the entrainment layer, above $z/z_i \sim 0.7$, the dimensionless gradients are represented by a family of curves. This indicates that the D scaling is ineffective in this domain. It can be noticed that the ''scatter'' in the figure is larger for the concentration points than that for the temperature points. This fact is due to the variation of the parameter Δc, ranging from negative to positive values in Table 1 (the parameter $\Delta\Theta$ varies in a relatively smaller interval).

Figure 7 presents the dimensionless gradients $G_{t\theta}^{(W)} \equiv (z_i/\Theta^*)\partial\Theta/\partial z$, and also $G_{tc}^{(W)} = (z_i/C^*)\partial c/\partial z$, obtained in performed LES experiments. The points in Fig. 8 are plotted for $z/z_i > 0.4$, to stress that the results represent the top-down diffusion processes. Functions $G_{t\theta}^{(W)}$ and $G_{tc}^{(W)}$ are of the order of 10^2 at the top of the mixed layer, and their scatter is substantial, especially for the concentration points. This clearly indicates that the W scaling is ineffective in the upper portion of the mixed layer.

The similarity functions $G_{tc} = (\Delta z/\Delta c)\partial c/\partial z$ and $G_{t\theta} = (\Delta z/\Delta\Theta)\partial\Theta/\partial z$ are shown in Fig. 8. They were obtained by normalizing gradients $\partial c/\partial z$ and $\partial\Theta/\partial z$ by their maximum values, by definition equal to $\Delta c/\Delta z$ and $\Delta\Theta/\Delta z$. Since the results represent the top-down processes, the data points in the figure are plotted for $z/z_i > 0.4$. For $z/z_i < 0.95$, the dimensionless gradients are unique functions of Z. They slightly diverge for $0.95 < z/z_i < 1.1$. Concentration and temperature points split above the mixed layer as a result of significant differences in the values of the Γ_c and Γ_θ. As can be noticed in Fig. 8, the scatter of the displayed points is reduced, in comparison to that in Figs. 6 and 7. This implies that the introduced top-down S scaling is effective.

The data points for the potential temperature and concentration are slightly shifted along the vertical axis. The maximum of the function G_{tc} occurs at about $z/z_i = 1.05$. Consequently, the parameter z_M can be estimated as equal to $1.05\ z_i$. The maximum of the function $G_{t\theta}$ is reached at about $z/z_i = 1.1$, which implies that $z_M = 1.1\ z_i$. The discrepancy between z_M for passive and active scalars seems to be an artifact caused by the initialization method for the concentration field (concentration calculations begin when temperature field is already in the quasi-steady state).

6. Similarity of scalars during free encroachment

The cloud-free, midday convective mixed layer is most often represented by the temperature profile and heat flux, schematically depicted in Fig. 1. The mixed layer can also exist in the state of free encroachment. In this section we will discuss how free encroachment differs from the bottom-up case depicted in Fig. 2a.

Free encroachment is characterized by a nil temperature gradient, and a zero heat flux at the top of the mixed layer. It occurs when the atmosphere above the morning mixed layer contains an isentropic layer, residual of the well-mixed layer from the previous day. When the surface temperature increases and reaches the temperature in the elevated isentropic layer, the mixed layer begins to grow into a neutrally stratified layer. The resulting regime lasts as long as it takes updrafts to travel from the actual mixed height to the top of the elevated isentropic layer, typically from several minutes to 1 h.

The initial potential temperature profile, during the free-encroachment run P00t, was assumed to be constant, and equal to 300 K in the 300-m deep mixed layer (Fig. 9). Above the mixed layer, there was a thin 90-m deep transition layer with a constant gradient, equal to

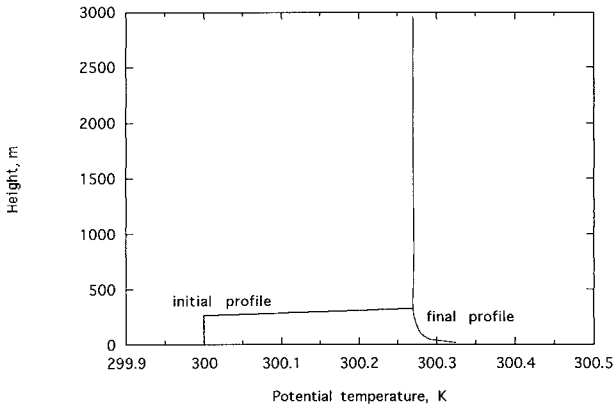

FIG. 9. Initial and final potential temperature profiles in run P00t (free encroachment).

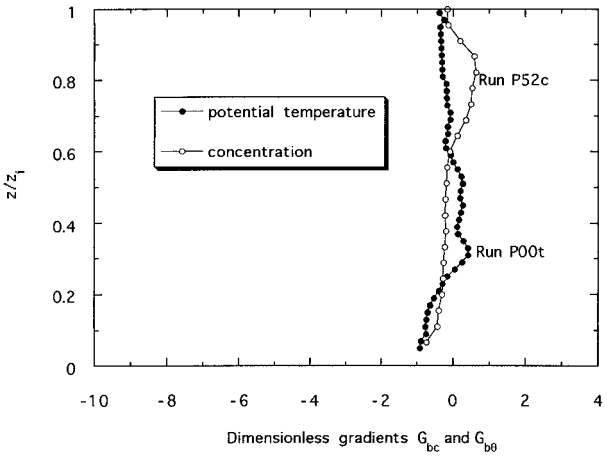

FIG. 10. Comparison of dimensionless gradients $G_{b\theta} = (z/\theta_f)\partial\Theta/\partial z$ in the free-encroachment run P00t, and $G_{bc} = (z/c_f)\partial c/\partial z$ in the bottom-up process in run P52c.

3 K km^{-1}. At the top, a nil temperature gradient was assumed. The heat flux at the earth's surface was kept constant, equal to 0.01 K m s^{-1}. During the simulation, the parameter $\Delta\Theta$ decreased in time, and eventually, the temperature in the mixed layer reached the potential temperature in the free atmosphere. At this moment, $\Delta\Theta = H_i = \partial\Theta/\partial z = 0$ at the top of the mixed layer. The resulting temperature profile is shown in Fig. 9.

Figure 10 presents the dimensionless gradient $G_{b\theta} = (z/\theta_f)\partial\Theta/\partial z$ in run P00T ($\Delta\Theta = 0$). In the same figure, dimensionless concentration gradient $G_{bc} = (z/c_f)\partial c/\partial z$, obtained in the pure bottom-up run P52c for concentration ($\Delta c = 0$, $\Delta\Theta > 0$), is also shown for comparison. The dimensional gradients, for both the potential temperature and concentration, are approximately equal. The differences between both functions in the figure are small, especially near the top of the mixed layer, where gradients do not diverge significantly from zero. For example, in Fig. 10, $G_{b\theta} = (z/\theta_f)\partial\Theta/\partial z$ is about 1 at $z/z_i = 0.8$ in run 52c, which after rescaling yields $\partial\Theta/\partial z \approx 0.03$ K km^{-1}. Differences near the lower surface are due to the numerical resolution and related limitations of the subgrid model in this region.

Figure 11 shows the heat flux in run P00t. The resulting heat flux is nonlinear in the upper half of the mixed layer. On the other hand, the concentration flux in run 52c is linear in the mixed layer (see Fig. 3). Consequently, the free-encroachment case differs from the pure bottom-up case depicted in Fig. 2a. The nonlinearity of the heat flux during free encroachment is due to the intense growth of the mixed layer into the neutrally stratified layer, with a zero gradient Γ_θ. This result clarifies the role of the temperature gradient Γ_θ, as the factor controlling a growth of the mixed layer. When Γ_θ is near zero, a nonsteady mixed layer is developed. When Γ_θ is large enough, the resulting mixed layer is a quasi-steady state with a linear heat flux profile. Because the nonlinearity of the heat flux in run P00t occurs in the upper portion of the mixed layer, where the temperature gradient is small, the universal form of $G_{b\theta}$ near the surface is not affected. Consequently, $G_{b\theta}$ nearly coincides with the dimensionless gradients G_{bc} obtained in run P52c (in which the concentration flux was linear).

7. Final remarks

The performed LES experiments demonstrate that for the purpose of the boundary layer parametrization, the gradient for a scalar concentration $g_c = \partial c/\partial z$ can be considered to be represented by two functions: $g_{bc} = \partial c_b/\partial z$ and $g_{tc} = \partial c_t/\partial z$; $g_c = g_{bc} + g_{tc} = G_{bc}c_f/z + G_{tc}\Delta c/\Delta z$, where G_{bc} and G_{tc} are the dimensionless scalar gradients. When the surface flux exists, the first function g_{bc} is large in the lower portion of the mixed layer and gradually decreases to zero with height. When the entrainment flux is present, the second function G_{tc} is substantial in the upper portion of the mixed layer and zero near the earth's surface. When the surface flux is nil (c_f

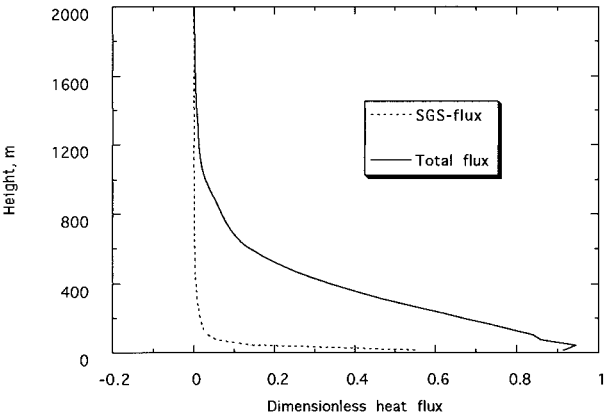

FIG. 11. Heat flux (total and subgrid) profiles obtained in run P00t (free encroachment).

$= 0$), g_{bc} contracts to zero. When the entrainment is eliminated ($\Delta c = 0$), g_{tc} is nil.

The decomposition $g_c = g_{bc} + g_{tc}$ is possible only for passive scalars, which do not affect turbulent flows in the mixed layer. Such a decomposition for the potential virtual temperature is not physical, since it is not realizable. Nevertheless, due to equality of dimensionless gradients of active and passive scalars ($G_{bc} = G_{b\Theta}$, $G_{tc} = G_{t\Theta}$), the gradient of the potential virtual temperature can also be expressed as a sum: $\partial\Theta/\partial z = G_{b\Theta}\Theta_f/z + G_{t\Theta}\Delta\Theta/\Delta z$.

The bottom-up diffusion is not confirmed by our simulations to be countergradient (i.e., G_{bc}, $G_{b\Theta} \to 0$ when $z \to z_M$). The top-down scaling (z_i, C^*, Θ^*), based on the values of entrainment fluxes, is found to be inefficient. Alternative scaling for concentration and for potential temperature is proposed using sets of ''bottom'' and ''top'' scales: (z, c_f, θ_f) and (Δz, Δc, $\Delta\Theta$). The bottom scaling consist of the classic free-convective scales. The top scales, based on the maximum values of the gradients in the interfacial layer, reduce the scatter of scalar gradients at the top of the boundary layer.

Acknowledgments. This research was sponsored by NSF Grant ATM 9217028. The author appreciates comments of Dr. Peter Sullivan and Dr. Bjorn Stevens.

APPENDIX

The LES Experiments

The employed LES model is based on a system of differential equations consisting of the conservation laws for momentum, air mass, passive scalar concentration, and the first law of thermodynamics. The list of unknown quantities includes three components of velocity, virtual potential temperature, passive scalar concentration, pressure, and the turbulent kinetic energy (TKE). The adopted subgrid parametrization is based on the TKE equation. Horizontal boundary conditions are assumed to be periodic. At the lower boundary, the vertical derivative of the turbulent kinetic energy is set to be zero. The Monin–Obukhov similarity formulation is employed to calculate surface momentum fluxes. The upper boundary condition is assumed to be stress free for horizontal velocity components. At the top of the computational domain, the vertical velocity is set to zero, and a zero TKE energy is assumed. The time and space increments are as follows: $\Delta t = 3$ s, $\Delta x = \Delta y = 50$ m, and $\Delta z = 30$ m. The mash consists of $64 \times 64 \times 60$ grid points. The geostrophic wind is assumed to be zero. The roughness length $z_0 = 0.1$ m, while the Coriolis parameter is assumed $f = 10^{-4}$. The wave-absorbing layer at the top of the computational domain is characterized by a timescale of 1000 s.

The performed experiments are summarized in Table 1. The symbols in the table can be identified as follows: z_i is the height of the mixed layer, Γ_θ is the temperature gradient in the free atmosphere (the concentration gradient Γ_c in the free atmosphere was assumed to be zero in all experiments), w^* is the convective scale for velocity, $\theta^* = H_0/w^*$ is the convective scale for temperature, $\Delta\Theta$ is the temperature ''jump'' in the interfacial layer, $R_\theta = H_i/H_0$ is the heat flux ratio at the top and the bottom of the mixed layer, $c^* = Q_0/w^*$ is the convective scale for concentration, Δc is the concentration jump in the interfacial layer, $R_c = Q_i/Q_0$ is the concentration flux ratio at the top and the bottom of the mixed layer, $t^* = z_i/w^*$ is the convective timescale, and T/t^* is the relative length of the simulation. Moreover, H_0 is the surface potential temperature flux and Q_0 is the passive scalar flux.

The table lists 11 experiments. The first experiment P00t was performed to study free encroachment ($\Delta\Theta = 0$). The second and the third experiments, P15b and P52c, were executed to generate pure top-down ($c^* = 0$) and pure bottom-up ($\Delta c = 0$) regimes for a passive scalar. The remaining simulations were designed to examine the bottom-up–top-down processes with $\Delta c < 0$ (runs P15a1, P30a, P30a1, P50a, and P60a) and with $\Delta c > 0$ (runs P15c, P30d, and P30c).

In the performed LES experiments, z_i was obtained in the range 615–855 m. The parameter Δz was in the range 80–100 m. The Richardson number $\mathrm{Ri} = \Delta\Theta/\theta^*$ was in the range from about 20 to 40. The range of Ri is controlled by the range of the potential temperature gradient in the free atmosphere Γ_θ, which varied from 1.5 to 5.0 K km^{-1}.

REFERENCES

Boers, R., 1989: A parametrization of the depth of the entrainment zone. *J. Appl. Meteor.*, **28,** 107–111.

Businger, J. A., J. C. Wyngaard, Y. Izumi, and E. F. Bradley, 1971: Flux profile relationships in the atmospheric surface layer. *J. Atmos. Sci.*, **28,** 181–189.

Deardorff, J. W., 1966: The counter-gradient heat flux in the lower atmosphere and in the laboratory. *J. Atmos. Sci.*, **23,** 503–506.

——, 1970: Convective velocity and temperature scales for the unstable planetary boundary layer and for Rayleigh convection. *J. Atmos. Sci.*, **27,** 1211–1212.

Lilly, D. K., 1968: Models of cloud-topped mixed layers under strong inversion. *Quart. J. Roy. Meteor. Soc.*, **94,** 292–309.

Mahrt, L., 1995: K-profile model and complications due to surface heterogeneity. *The Planetary Boundary Layer and Its Parameterization*, C.-H. Moeng, Ed., NCAR.

Moeng, C.-H., and J. C. Wyngaard, 1984: Statistics of conservative scalars in the convective boundary layer. *J. Atmos. Sci.*, **41,** 3161–3169.

Monin, A. S., and A. M. Obukhov, 1954: Basic laws of turbulent mixing in the atmosphere near the ground. *Tr. Geofiz. Inst., Akad. Nauk SSSR*, **151,** 163–187.

Nieuwstadt, F. T. M., 1984: The turbulent structure of the stable, nocturnal boundary layer. *J. Atmos. Sci.*, **41,** 2202–2216.

Piper, M., J. C. Wyngaard, W. H. Snyder, and R. E. Lawson Jr., 1995: Top-down, bottom-up diffusion experiments in a water convection tank. *J. Atmos. Sci.*, **52,** 3607–3619.

Sorbjan, Z., 1986: On similarity in the atmospheric boundary layer. *Bound.-Layer Meteor.*, **34,** 377–397.

——, 1988a: Structure of the stably-stratified boundary layer during

the SESAME-1979 experiment. *Bound.-Layer Meteor.,* **44,** 255–266.

——, 1998b: Local similarity of spectral and cospectral characteristics in the stable-continuous boundary layer. *Bound.-Layer Meteor.,* **35,** 257–275.

——, 1989: *Structure of the Atmospheric Boundary Layer*. Prentice Hall, 317 pp.

——, 1995: Toward evaluation of heat fluxes in the convective boundary layer. *J. Appl. Meteor.,* **34,** 1092–1098.

Stull, R., 1976: The energetics of entrainment across a density interface. *J. Atmos. Sci.,* **33,** 1260–1267.

Weil, J. C., 1990: A diagnosis of the asymmetry in top-down and bottom-up diffusion using a Lagrangian stochastic model. *J. Atmos. Sci.,* **47,** 501–515.

Wyngaard, J. C., 1984: Toward convective boundary layer parametrization: A scalar transport module. *J. Atmos. Sci.,* **41,** 1959–1969.

——, 1987: A physical mechanism for the asymmetry in the top-down and bottom-up diffusion. *J. Atmos. Sci.,* **44,** 1959–1969.

——, and R. A. Brost, 1984: Top-down and bottom-up diffusion of a scalar in the convective boundary layer. *J. Atmos. Sci.,* **41,** 102–112.

Zilitinkevich, S. S., and D. V. Chalikov, 1968: On estimation of vertical turbulent fluxes in the atmospheric surface layer based on gradient observations (in Russian). *Izv. AN SSSR, Fiz. Atmos. Okeana,* **4,** 915–929.